Research in Astronomy and Astrophysics, 22:075009 (10pp), 2022 July https://doi.org/10.1088/1674-4527/ac712a
© 2022. National Astronomical Observatories, CAS and IOP Publishing Ltd. Printed in China and the U.K.

Pulsar Survey With the QiTai 110 m Radio Telescope

Xie Jintao[1,2], Wang Jingbo[1,3,4], Wang Na[1,3,4], and Hu Yue[1]
[1] Xinjiang Astronomical Observatory, Chinese Academy of Sciences, Urumqi 830011, China; wangjingbo@xao.ac.cn, na.wang@xao.ac.cn
[2] University of Chinese Academy of Sciences, Beijing 100049, China
[3] Key Laboratory of Radio Astronomy, Chinese Academy of Sciences, Urumqi 830011, China
[4] Xinjiang Key Laboratory of Radio Astrophysics, Urumqi 830011, China
Received 2021 August 23; revised 2022 April 13; accepted 2022 May 12; published 2022 June 14

Abstract

With a collecting area of 9400 m^2, the Xinjiang QiTai 110 m radio Telescope (QTT) will allow for a significant advance in the search and observation of pulsars. We have updated the galactic electron density model, scattering model, spectral distribution, and radial distribution of PSRPOPPY to generate the population of isolate radio pulsars in the Galaxy. The spiral arm, including the local spiral arm, is considered when generating pulsar locations. By simulation, we estimate the number of previously undetected radio pulsars that QTT will discover with its possible receivers for different strategies. Using the PAF receiver, 2200 previously unknown pulsars could be discovered in 43 days. The 96-beam PAF receiver can produce ∼10.56 GB of data per second.

Key words: (stars:) pulsars: general – Galaxy: structure – telescopes

1. Introduction

The 110 m QiTai radio Telescope (QTT) is planned to be built in Qitai, Xinjiang Uygur Autonomous Region, China. QTT will be one of the world-leading scientific facilities and the world's largest fully steerable radio telescope. With a minimum elevation angle of 7°, QTT covers ∼85% of the entire sky (Wang 2014). It will be equipped with a suite of ultra-wide bandwidth (UWB) receivers and Phased Array Feed (PAF) and operated at frequencies ranging from 150 MHz to 115 GHz. Taking advantage of its sensitivity and capacity of sky coverage, QTT has outstanding potential in discovering unknown radio pulsars. In addition, QTT will provide high-quality pulsar timing data, which will significantly impact various fields of astrophysics.

Radio pulsars are intriguing celestial objects, which offer insights into a wide variety of astrophysics and physics, including the study of the interstellar medium, globular clusters, the formation and evolution of binary systems, the evolution of massive stars, testing theories of gravity, the magnetic field of the Galaxy, extreme plasma physics, the properties of super-dense matter (Lorimer & Kramer 2005). Since the first pulsar was discovered (Hewish et al. 1968), pulsars have been continued search for more than 50 yr. Over 2600 normal radio pulsars and 455 millisecond pulsars (MSPs) have been discovered (see ATNF[5] Pulsar Catalogue V1.65; Manchester et al. 2005). Several peculiar pulsars have been found for the last few decades, including the double pulsar system (see e.g., Burgay et al. 2003; Lyne et al. 2004), Magnetar (Kaspi et al. 2004), millisecond pulsar in a stellar triple system (Ransom et al. 2016), and rotating radio transients (McLaughlin et al. 2006).

The goal of the paper is to study the ability of QTT to discover new radio pulsars. In Section 2, we outline models used to generate simulated populations in the Galaxy. In Section 3, we present simulations of pulsar survey with QTT, where we calculate the time it takes to complete a pulsar survey and the number of unknown pulsars that can be detected for different receivers. In Section 4, we estimate the data rates with different bandwidths and observing frequencies for a pulsar survey with QTT. Section 5 contains a discussion of the results as well as the synergy with FAST.

2. Population Synthesis of Isolate Radio Pulsars in the Galaxy

PSRPOPPY (Bates et al. 2014) is an open-source package written in Python2, developed from PSRPOP (Lorimer et al. 2006). It can be used to study pulsar population (Huang & Wang 2020) and predict the results of future pulsar surveys (e.g., Keane et al. 2015). As support for Python2 was terminated on 2020 January 1, we upgraded PSRPOPPY to Python3.

We used 1316 normal pulsars, and 61 MSPs from a series of Multibeam Pulsar Surveys (MBPS) conducted at Parkes to derive an underlying pulsar population. These surveys included Parkes (Manchester et al. 2001), Swinburne (Edwards et al. 2001), high latitude (Burgay et al. 2006), and Perseus Arm (Burgay et al. 2013) Multibeam Pulsars Surveys.

To generate simulated pulsar populations, we updated the spectral index distribution, the galactic electron density model, pulsars radial distribution (Xie et al. 2022), the method for

[5] https://www.atnf.csiro.au/research/pulsar/psrcat/

generating pulsar locations, and scatter model in PSRPOPPY. Other parameters are default setting of PSRPOPPY. The details are given below.

2.1. Spectral Index Distribution

The pulsar spectral index distribution is necessary to scale the derived luminosity of a simulated pulsar at a particular frequency to another frequency. The default spectral index distribution given by PSRPOPPY is a Gaussian distribution with a mean value of $\alpha = -1.6$ and a standard deviation of $\sigma = 0.35$ (Lorimer et al. 1995).

Jankowski et al. (2018) presented the largest sample of absolute calibrated pulsar flux density measurements to date. These multi-frequency and high-sensitivity observations provide a uniform, systematic sample of pulsar flux densities. They obtained the weighted mean spectral index of $\alpha = -1.6$ by studying the spectral properties of 441 pulsars. To scale the luminosity at 1400 MHz to other frequencies, we assume that the spectra of pulsars are power-law (Lorimer et al. 1995) and assign a spectral index of simulated pulsar drawn from a Gaussian distribution with a mean of $\alpha = -1.6$ and standard deviation $\sigma = 0.54$ (Jankowski et al. 2018).

2.2. Spatial Distribution

In the simulation, an updated radial distribution is used (Xie et al. 2022). The radial distribution is derived from pulsars discovered by the MBPS survey, and the consistency of MBPS survey sensitivity can generate a more accurate radial distribution function. The distances of pulsars are estimated from the electron density model (Yao et al. 2017; hereafter YMW16), which is consistent with the electron density model used in the simulation so that better simulation results can be obtained.

The pulsar radial distribution function is as follows:

$$\rho(r) = A\left(\frac{r + R_{\rm pdf}}{R_\odot + R_{\rm pdf}}\right)^a \exp\left[-b\left(\frac{r - R_\odot}{R_\odot + R_{\rm pdf}}\right)\right], \quad (1)$$

where $R_\odot = 8.3$ kpc is the Sun-GC distance, $A = 23.09 \pm 0.24$ kpc^{-2}, $a = 12.38 \pm 3.05$, $b = 18.14 \pm 3.66$, $R_{\rm pdf} = 6.47 \pm 1.33$. As shown in Figure 1, the positions of pulsars are highly associated with the spiral arms. On the other hand, the positions of pulsars can be simply divided into two components, within and outside Galaxy's central region. The region outside the galactic center can be divided into five parts according to the spiral arms described by Equation (2), and the spiral arm parameters are shown in Table 1.

$$\theta = \ln\left(\frac{r}{r_0}\right) \Big/ \tan(\theta_1) + \theta_0, \quad (2)$$

Thus, the Galaxy is simply divided into six regions: the Galaxy Center, Norm arm, Perseus arm, Carina-Sagittarius arm, Crux-Scutum arm, and Local arm.

To generate positions of simulated pulsars, we need to make the simulated pulsar fall on a selected region with a certain probability. First, the ratio of pulsars in the two regions can be determined by integrating the inner and outer regions of the Galaxy center using Equation (1). Then, the area outside the galactic center is divided into five parts according to the spiral arms. The ratio of pulsars in each spiral arm can be obtained by integrating along the spiral arm with the radial distribution function. The proportions of pulsars in the galactic center and each spiral arm are shown in Table 2. For pulsars in the galactic center region, the distance from the galactic center and the galactic longitude l are generated by two independent random processes. According to the radial distribution function and the distance between the galaxy center and the pulsar, the probability of the distance between the galaxy center of the pulsar can be obtained as follows:

$$P(r) = 2 \times 10^{-7} \pi r \rho(r), \quad (3)$$

where $\rho(r)$ is the pulsars density on the Galactic plane, r is the distance of the simulated pulsar from the galactic center. The galactic longitude of simulation pulsar is randomly chosen in the interval $[0, 2\pi)$ rad. According to the method described by Xie et al. (2022), their positions were generated for pulsars in the spiral arm. The distribution of simulated pulsars in the galaxy is shown in Figure 2.

2.3. Electron Density Model of the Galaxy

Yao et al. (2017) presented a new model for the distribution of free electrons in the Galaxy with a more realistic spiral arm structure. We replace NE2001 with the YMW16 model in PSRPOPPY to estimate the pulsar dispersion measure (DM). Using the structure model of the Galaxy, the radial distribution of pulsars in the Galaxy, and pulsars distribution in the galactic Z direction, we get the position of the simulated pulsar in the Galaxy and the distance from the solar system. The simulated pulsar DM is mainly estimated from the galactic electron density model and distance. It is crucial to get a befitting of DM, which strongly affects detection sensitivity. We use the YMW16 electron density model to compute the expected dispersion measure and scatter broaden effects on each simulated pulsar.

2.4. Scattering Effect

The sensitivity of a pulsar survey can be estimated by the minimum detectable flux density $S_{\rm min}$, which is mainly related to the performance of the telescope, pulsar period, pulse width, and sky background temperature. $S_{\rm min}$ of a simulated pulsar in a

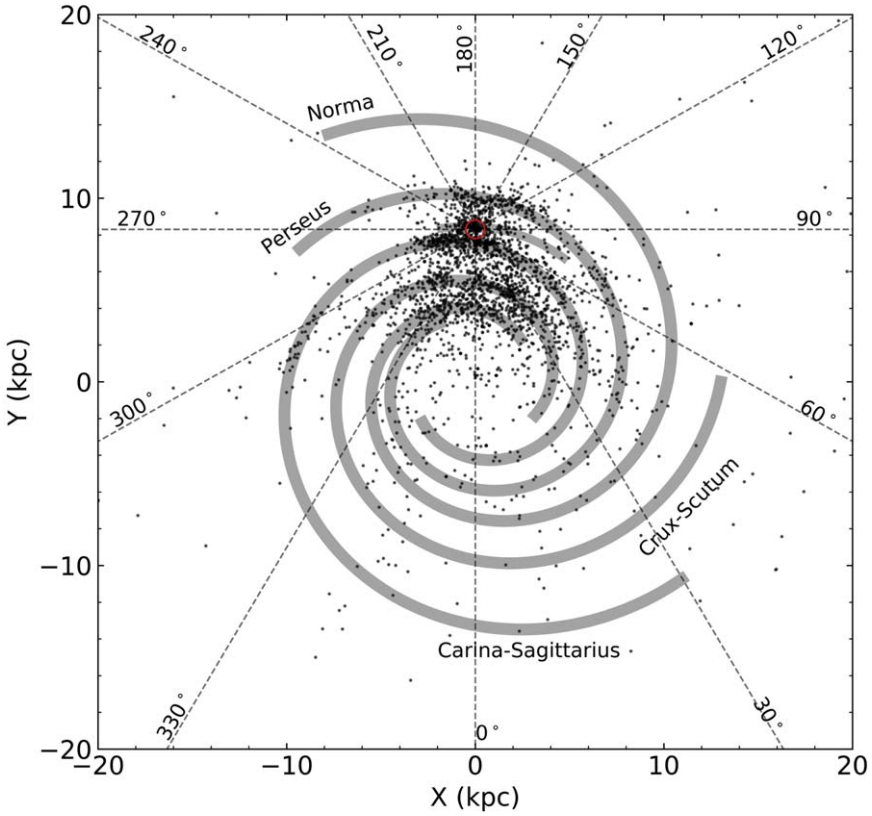

Figure 1. The distribution of pulsars on the galactic plane. The red circle is the position of the solar system. The Hou & Han (2014) model was used for the spiral arm parameters of the Galaxy.

Table 1
Spiral Arm Parameters

Arm Number	Name	θ_0 (deg)	θ_1 (deg)	r_0 (kpc)
1	Norm	44.4	11.43	3.35
2	Perseus	120.0	9.84	3.71
3.	Carina-Sagittarius	218.6	10.38	3.56
4	Crux-Scutum	330.3	10.54	3.67
5.	Local arm	55.1	2.77	8.21

Table 2
The Proportion of Pulsars in the Composition of the Galaxy

Arm Number	Name	Ratio (%)
1	Galaxy Center	17.09
2	Norm	19.41
3	Perseus	20.34
4	Carina-Sagittarius	20.75
5	Crux-Scutum	19.69
6.	Local arm	2.81

specific survey can be expressed as:

$$S_{\min} = \frac{\alpha\beta T_{\rm sys}}{G\sqrt{N_{\rm p}Bt_{\rm obs}}}\left(\frac{W_{\rm eff}}{P - W_{\rm eff}}\right)^{\frac{1}{2}}, \quad (4)$$

where α is the threshold signal-to-noise ratio (SNR) above which a pulsar can be detected (9 in our case); β is degradation factor; $T_{\rm sys}$ is the radio telescope system temperature (K); G is the telescope gain (K/Jy); N_p is the number of polarization; $t_{\rm obs}$ is dwell time per pointing; B is the bandwidth (MHz) of the receiver when observing a pulsar; P is the pulse period of an observed pulsar (s); $W_{\rm eff}$ is the effective pulse width. As shown by the following equation, DM contributes a lot to broad pulse width.

$$W_{\rm eff} = \sqrt{W_{\rm int}^2 + t_{\rm samp}^2 + \Delta t^2 + \tau_{\rm sc}^2}, \quad (5)$$

where $W_{\rm int}$ is the pulsar intrinsic pulse width, $t_{\rm samp}$ is the sampling time when recording the data, and Δt is the scattering pulse smearing caused by the ionized interstellar medium. Bhat et al. (2004) measured pulse broadening due to the scattering

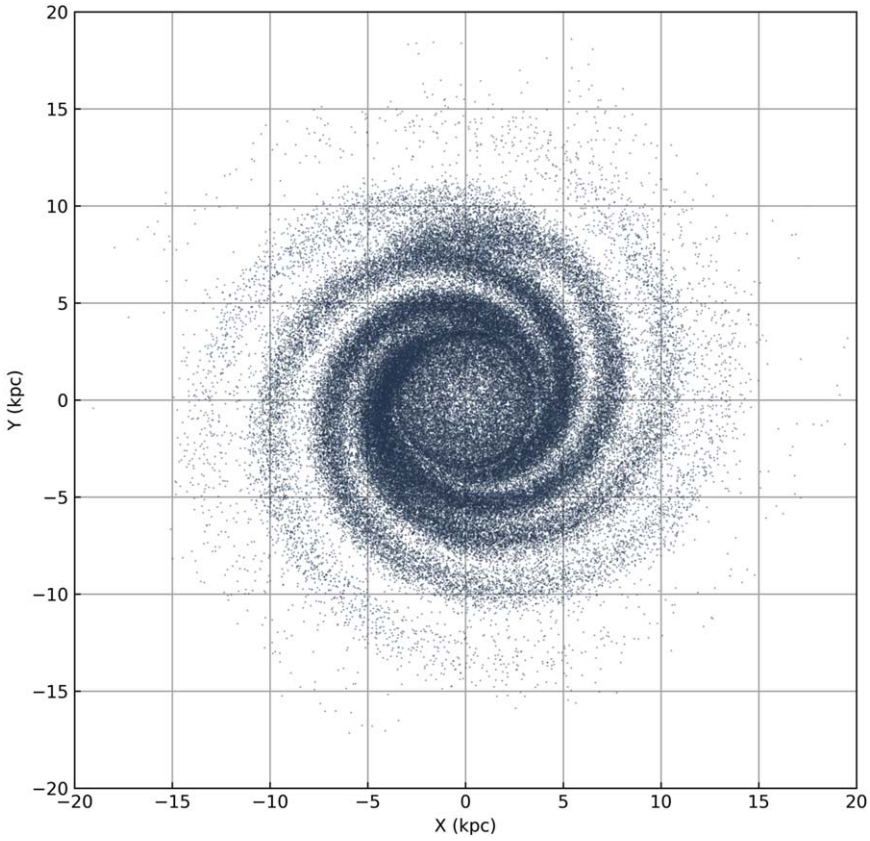

Figure 2. Simulation of isolate normal radio pulsars distribution in the Galactic plane.

effect and fit $\tau_{\rm sc}$ and DM using a simple equation:

$$\log_{10}\tau_{\rm sc} = -6.46 + 0.154\log_{10}{\rm DM} + 1.07(\log_{10}{\rm DM})^2 - 3.86\log_{10}f_{\rm GHz}, \quad (6)$$

for a pulsar with a certain dispersion measure, τ_{sc} is at the observed frequency $f_{\rm GHz}$. Krishnakumar et al. (2015) fit the empirical relation of $\tau_{\rm sc}$ and DM as shown

$$\tau_{\rm sc} = 3.6\times10^{-6}{\rm DM}^{2.2}(1.0 + 1.94\times10^{-3}{\rm DM}^{2.0}) \times\left(\frac{f_\nu}{327\ {\rm MHz}}\right)^{-4.0}, \quad (7)$$

We added both scattering models into PSRPOPPY and compared the generated pulsar populations. There was no significant difference found between the two populations. To be consistent with the scattering model used in the electron density model YMW16, we adopt the functional form of Krishnakumar et al. (2015).

After all the updates were added into PSRPOPPY, simulated pulsar populations with ∼100,000 normal pulsars and ∼28,000 millisecond pulsars were generated.

Table 3
The Expected System Parameters of QTT

Receiver	15 cm	40 cm	PAF
Gain (K/Jy)	2.06	1.89	2.24
System temperature (K)	15	20	20
Bandwidth (MHz)	3300	1530	1100
Frequency range (MHz)	700–4000	270–1800	700–1800
No. of beams	1	1	96

3. Pulsar Survey Simulation with QTT

In the past decades, several extensive pulsar surveys have been completed (see e.g., Manchester et al. 1996; Lyne et al. 1998; Manchester et al. 2001; Keith et al. 2010). There are also many ongoing surveys (see e.g., Stovall et al. 2014; Sanidas et al. 2019; Han et al. 2021). With an excellent geographical location and observational environment, QTT can search for pulsars with high sensitivity in the Northern Hemisphere. Table 3 presents the parameters involved in the survey simulation.

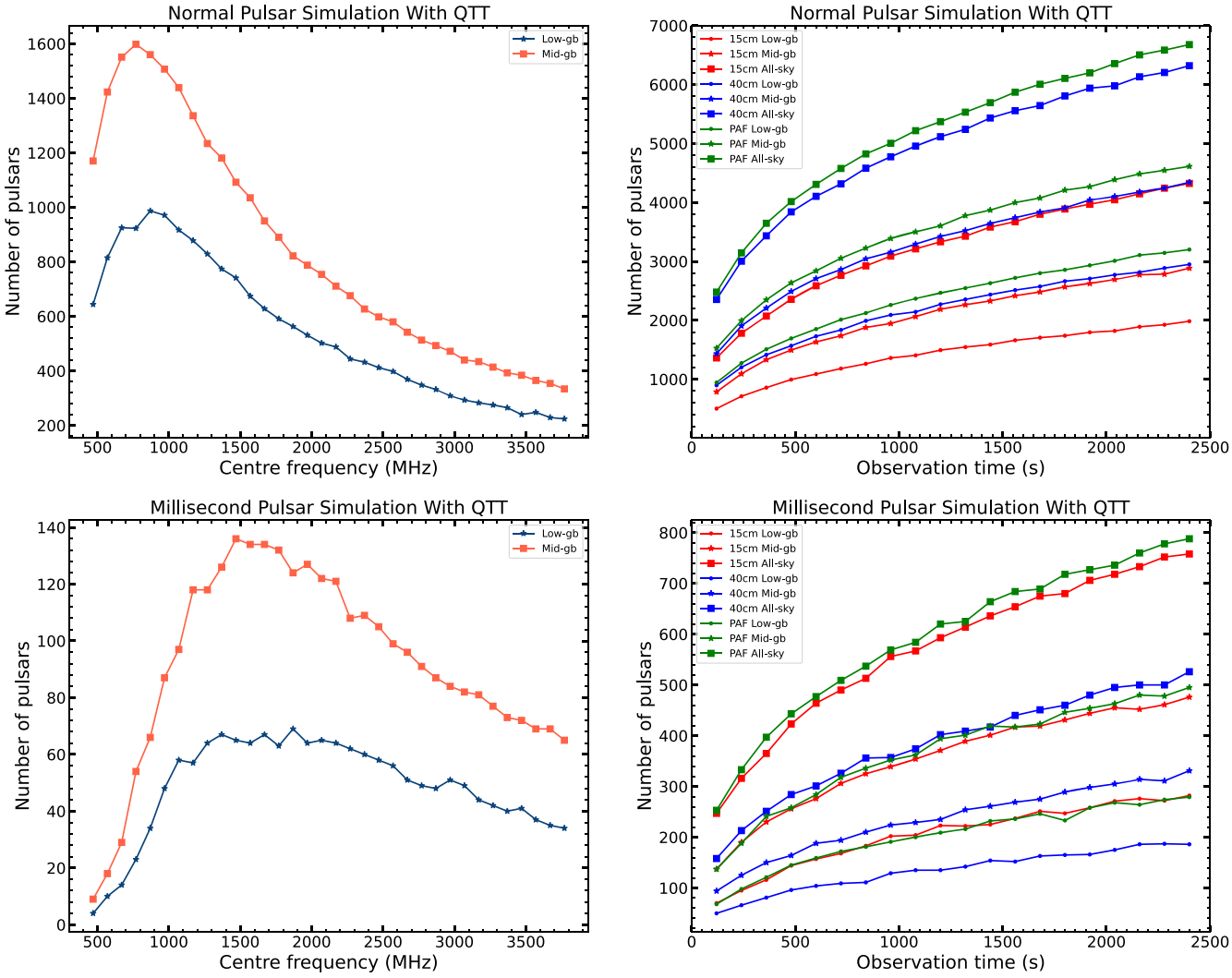

Figure 3. Left: the number of pulsars detected in the simulation of QTT surveys versus observations frequency. Right: the number of pulsars detected in the simulation of QTT surveys as a function of observation time. Low-gb and Mid-gb indicate $|b| < 5°$ and $|b| < 10°$, respectively.

Many factors could affect pulsar survey, such as sky background radiation, observation frequency, observation duration. After the pulsar population was generated through simulation, we can use the parameter of the QTT receiver to simulate the pulsar survey, to find the relationship between the number of detected pulsars and observation duration and frequency. QTT will be equipped with three receivers for pulsar observation, including a 15 cm receiver, 40 cm receiver, and phased array feed receiver. Table 3 shows the parameters of receivers (Ma et al. 2019). According to the receiver parameters, we can perform the simulated pulsar survey in different galactic regions with different parameters. These parameters include bandwidth, frequency, observation duration, and field of view (FoV), where FoV is related to observation frequency. It is not easy to define the field of view for the wideband receiver. Calculating FoV with the center frequency of the UWB receiver will result in more pointing of the survey coverage but ensure that the pulsar survey's sensitivity will not be lost too much. Therefore, the center frequency of the receiver is used to calculate FoV in this paper. The channel bandwidth and sampling time were set as 0.1 MHz and 50 μs, respectively.

The pulsar observation frequency of QTT is from ∼270 MHz to ∼4000 MHz. Once the pulsar population was generated, we performed simulations to find the number of pulsars QTT would detect as a function of frequency. For this purpose, we allowed the center frequency to range from 470 MHz to 3770 MHz with a constant bandwidth of 200 MHz. The system temperature at the frequency band edge of the receiver is relatively high, which is usually cut off in the

Table 4
QTT Pulsar Survey Parameters and Corresponding Simulation Results

Parameter	Mode 1	Mode 2	Mode 3	Mode 4	Mode 5	Mode 6	Mode 7	Mode 8
Receiver	40 cm	40 cm	40 cm	40 cm	PAF	PAF	PAF	PAF
Survey regions	$\|b\| < 5°$	$\|b\| < 10°$	$\|b\| < 5°$	$\|b\| < 10°$	$\|b\| < 5°$	$\|b\| < 10°$	$\|b\| < 5°$	$\|b\| < 10°$
Pointing time (s)	720	720	1800	1800	720	720	1800	1800
Bandwidth (MHz)	1530	1530	1530	1530	1100	1100	1100	1100
Number of beams	1	1	1	1	96	96	96	96
Number of normal pulsars detected	2160	2772	3051	3850	2322	2965	3327	4126
Number of MSPs detected	137	184	204	280	207	290	292	420
Currently known normal pulsars in region	1080	1172	1080	1172	1080	1172	1080	1172
Currently known MSPs in region	240	193	240	193	240	193	240	193
Total survey time (12 hour days)	708	1372	1770	3430	17	33	43	83

process of data processing. So the band edge (∼4 percent) is not considered. The number of pulsars that QTT can detect in different frequency bands is shown in Figure 3. With ∼85% coverage of the whole sky, QTT will be able to complete pulsar surveys with very high sensitivity. Considering the sky coverage of QTT, we divided the pulsar survey into two types. One contains only low Galactic latitude b, with a Galactic latitude range of $\pm 5°$ and a longitude range of $[-5°, 180°]$. The other contains low and medium latitudes, with a latitude range of $\pm 10°$ and a Galactic longitude range of $[0°, 180°]$. The number of pulsars found included known pulsars in all the simulations.

Assuming the bandwidth of 1530 MHz, the FoV of the 40 cm receiver is 0.0435 deg^2. The PAF receiver has 96 beams with an FoV of 1.795 deg^2 at the center frequency of 1250 MHz. Using the FoV of the receiver, we calculated the total observing time required for QTT to complete the pulsar survey with different observation lengths per pointing and different survey regions, as shown in Table 4. We assume that the observing time for the pulsar survey is 12 hours per day.

As shown in Figure 3, the optimal survey frequency for millisecond pulsars is significantly higher than for normal pulsars. The main reason is that millisecond pulsars' period and pulse width is different from normal pulsars. The number of pulsars detected by QTT is positively correlated with the observation time. Furthermore, this trend is more evident for large-scale pulsar surveys and millisecond pulsars. In addition, we find that the number of pulsars that can be detected is not simply proportional to the receiver bandwidth.

With wider bandwidth, the 15 cm receiver does not perform as well as the other two receivers in simulating the search for normal pulsars within the same sky coverage. The main reason is that Equation (4) is not suitable to estimate minimum detectable flux density for the UWB receiver. The spectral of most pulsars can be describe as a simple power law with average spectral index of about −1.6 (Jankowski et al. 2018). Pulsar flux density decreases rapidly with the increasing observing frequency. Therefore, for UWB receivers, the low-frequency part contributes much more than the high-frequency part. The number of detectable pulsars is underestimated using the UWB receiver's center frequency in the simulation. To estimate the actual minimum detectable flux density of the UWB receiver, lower center frequency and narrower bandwidth need to be used in Equation (4). To explore the capability of the 15 cm receiver in searching pulsar, we simulated pulsars that can be detected by the 15 cm receiver with different center frequencies and bandwidths, as shown in Figure 4. With the 15 cm receiver from 700 MHz to 2700 MHz, QTT can find at least 3000 pulsars near the galactic plane ($-5° < l < 180°$ and $|b| < 5°$). When searching for millisecond pulsars, the 15 cm receiver performs better than the 40 cm receiver because of the reduced influence of background radiation and dispersion smearing at high frequencies.

We perform a simulation of the pulsar survey with QTT using 40 cm and PAF receivers in different Galactic regions. The surveys were limited in Galactic latitude and longitude by $|b| < 5°$ or $|b| < 10°$ (more than 70% of known pulsars are in this region). The observation time per pointing was constant at 720 s or 1800 s. Using the 40 cm receiver, QTT can find about 800 undiscovered pulsars near the galactic plane ($-5° < l < 180°$ and $|b| < 5°$) in about 708 days. About 2200 previously undetected pulsars can be discovered in 43 observing days using the PAF receiver with 30 minutes pointing. Expanding the survey area to $|b| < 10°$ will add about 600 unknown radio pulsars with 12 minutes pointing and about 850 pulsars with 30 minutes pointing.

4. Data Processing

The total amount of data generated by the pulsar survey is related to many parameters, including the bandwidth B, observation duration per pointing $t_{\rm obs}$ (s), the sampling interval $t_{\rm samp}$ (s), the entire field of the survey $\Omega_{\rm survey}$, the field of view of one beam $\rm FoV_{beam}$, the number of beams $N_{\rm beam}$, sampling bit number used in the digitization $N_{\rm bit}$, and the number of

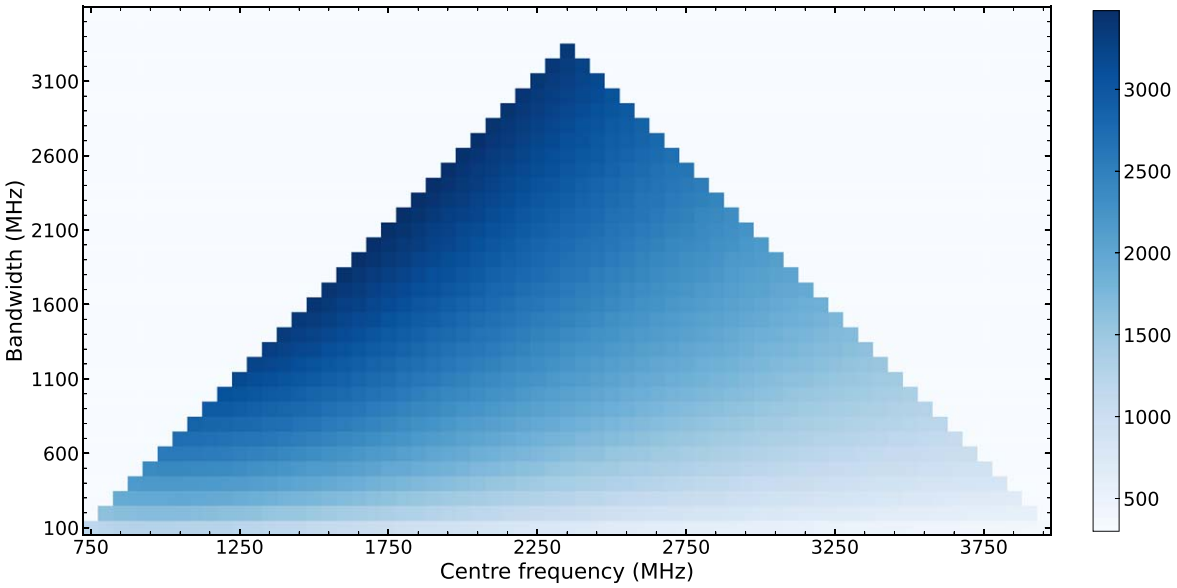

Figure 4. The number of detected pulsar for the simulated QTT pulsar survey with different center frequencies and bandwidths. The observation duration is 720 s. The color represents the number of detected simulated pulsars.

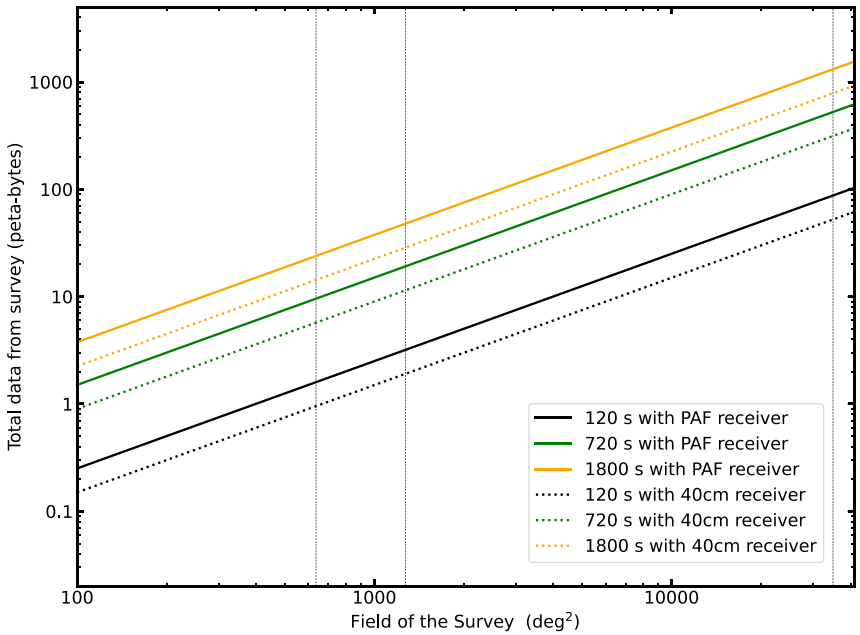

Figure 5. The total amount of data from a QTT pulsar survey as a function of the total survey field with a bandwidth of 1100 MHz, two polarizations, and 8 bits per sample. The FoV_{beam} of PAF and 40 cm receiver are 0.0187 deg^2 and 0.0435 deg^2 respectively. 40 cm receiver is indicated by dashed lines. The solid lines represent the PAF receiver. The black line, green line, and yellow lines correspond to observation times of 120 s, 720 s and 1800 s. The dotted vertical lines indicate from left to right the survey fields given by $-10^\circ < l < 90^\circ$, $|b| < 5$ and $-10^\circ < l < 90^\circ$, $|b| < 10$, and the entire visible sky.

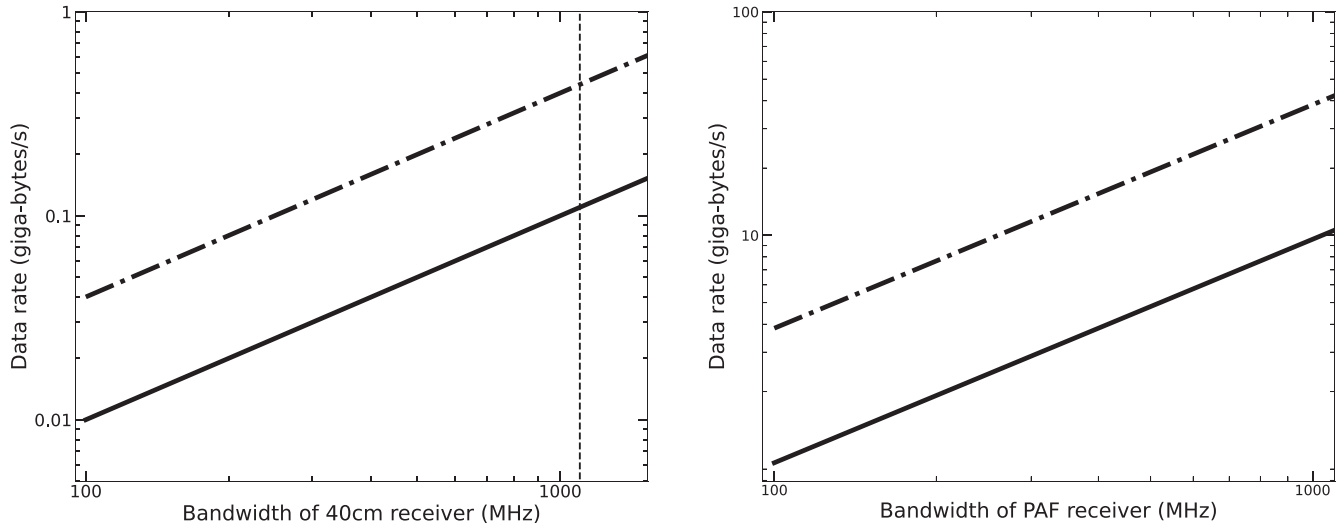

Figure 6. Data acquisition rate from a QTT pulsar survey as a function of bandwidth for PAF receiver and 40 cm receiver. The vertical curve indicates a bandwidth of 1100 MHz. The solid line is sampled at 2 bits, and the dotted-dashed line is sampled at 8 bits. For the PAF receiver, we assume a sampling interval of 50 μs, a bandwidth range of 100–1100 MHz, the number of beams is 96. The 40 cm receiver has a bandwidth range of 100 MHz–1530 MHz and a single beam.

polarization $N_{\rm pol}$. It is given by

$$D_{\rm total} = \frac{B}{\Delta v}\frac{t_{\rm obs}}{t_{\rm samp}}\frac{\Omega_{\rm survey}}{{\rm FoV}_{\rm beam}}N_{\rm pol}\frac{N_{\rm bit}}{8}\ {\rm Byte} \quad (8)$$

Figure 5 shows the total amount of data from a QTT pulsar survey as a function of the entire survey field for different observation times. We have assumed an ${\rm FoV}_{\rm beam}$ of 0.0187 deg^2 for PAF receiver, ${\rm FoV}_{\rm beam}$ of 0.0435 deg^2 for 40 cm receiver, a bandwidth of 1100 MHz, $\Delta v = 0.1$ MHz, a sampling interval of $t_{\rm samp} = 50\ \mu$s, $N_{\rm pol} = 2$ and $N_{\rm bit} = 8$. For the PAF receiver, assuming an observation time of 1800 s, the all-sky survey would produce 1313 peta-bytes of data. A large number of files will be generated when we process the data, which also requires a large amount of disk space. In addition, the observation time per pointing of 2 minutes, 12 minutes, and 30 minutes was considered. Another critical challenge is to balance channel bandwidth Δv and data acquisition rate. For a given total bandwidth B and channel bandwidth, the data acquisition rate of the filterbank output can be expressed as:

$$D_{\rm rate} = \frac{N_{\rm beams}}{t_{\rm samp}}\frac{B}{\Delta v}\frac{N_{\rm bit}}{8}N_{\rm pol}\ {\rm Bps} \quad (9)$$

where $t_{\rm samp}$ is the sampling interval and $N_{\rm bit}$ is the number of bits used in the digitization. The effective time resolution and dispersion smearing can be used to constrain channel bandwidth, which is given by the sampling interval and pulse smearing $t_{\rm scatt}$ due to the scattering:

$$\Delta v({\rm GHz}) \leqslant \frac{\sqrt{t_{\rm samp}(\mu{\rm s}) + t^2_{\rm scatt}(\mu{\rm s})}\, v^3_{\rm min}\,({\rm GHz})}{8.3\times 10^3\ {\rm DM}} \quad (10)$$

In practice, the pulse smearing due to the scattering can differ from Equation (6) by a factor up to 100 (Bhat et al. 2004). We compared the scattering models of Krishnakumar et al. (2015) and Bhat et al. (2004), and the differences are within an order of magnitude. For a pulsar survey, it is necessary to minimize the effects of scattering, which requires a narrow channel bandwidth. We calculated the scattering time at the lowest frequency of the receiver and divided the result by 100 to avoid missing any pulsars due to scattering. By applying the scattering time $t_{\rm scatt}$ and the minimum frequency $v_{\rm min}$ of the receiver to Equation (10), we can obtain the channel bandwidth Δv required for observation at a given DM. Since no more than 10% of pulsars have DM greater than 498, we set DM to 498. It means that the channel bandwidth of 4.19 kHz is sufficient for the PAF receiver and 1.55 kHz for the 40 cm receiver for the pulsar survey; this leads to 987,097 frequency channels for the 40 cm receiver with a bandwidth of 1530 MHz and 262,530 frequency channels for PAF receiver with 1100 MHz, respectively. However, it may not be necessary to set up so many frequency channels in an actual pulsar survey. The smallest channel bandwidth of existing surveys at similar frequency is about 0.1 MHz, such as Arecibo 327 MHz Drift-Scan Pulsar Survey (Martinez et al. 2019) and FAST Galactic Plane Pulsar Snapshot survey (Han et al. 2021), which found many millisecond pulsars with short periods. Figure 6 shows the data rate of a QTT pulsar survey as a function of the bandwidth. We have assumed 50 μs sampling interval, a frequency range of 0.27 to 1.8 GHz, two polarizations, a channel bandwidth of 0.1 MHz, and 2-bits per sample. For the 40 cm receiver with a bandwidth of 1530 MHz, the data rate is about 0.153 GB per second, and 0.612 GB/s with 8-bit

sampling. For the PAF receiver with 2-bits per sample, the data rate is about 10.56 GB per second. If 8-bit sampling is used, the data rate will be 42.24 GB per second.

The number of operations per second required for searching pulsars from these data is approximately

$$N_{os} = N_{\rm beam} N_{\rm DM} N_{\rm acc} \times 5 N_{\rm samp} \log_2(N_{\rm samp})/t_{\rm obs}, \quad (11)$$

where $N_{\rm beam}$ is the number of beams, $N_{\rm DM}$ is the number of DM-trial values, and $N_{\rm acc}$ is the number of trial accelerations. For the QTT pulsar survey with the 40 cm receiver, we assumed that observation duration per pointing ($t_{\rm obs}$) is 720 s, the sampling time is 50 μs, the $\rm DM_{max}$ is 1000 $\rm cm^{-3}$ pc, and the number of trial accelerations is 100. $N_{\rm DM}$ can be calculated using DDPLAN.PY from PRESTO. Assuming that the bandwidth is 1530 MHz and the channel bandwidth is 0.1 MHz, $N_{\rm DM}$ is 48,845, resulting in 11.6 tera-ops of required computation power for real-time analysis. For the PAF receiver with 96 beams, it will be 675.3 tera-ops. The number of operations increased by de-dispersion, harmonic folding, and other processes will double the above number of operations at most. While it is not unreasonable to process data from QTT pulsar surveys offline, it still requires enormous computing and storage resources.

5. Discussion and Summary

We have updated the galactic electron density model, scattering model, spectral exponential distribution, and pulsar radial distribution model of PSRPOPPY and generated pulsar population in the Galaxy. The Galaxy is divided into six parts that could make pulsars' position close to the actual situation. The simulations show that there are about 10,000 pulsars that can be observed in the Galaxy. Moreover, we calculate the proportion of pulsars in each part of the Galaxy. Pulsars near the Local Arm account for only 2.81% of all pulsars in the Galaxy. By comparing Figures 1 and 2, we found that there are still a large number of pulsars in other spiral arms that have not been detected. Our simulation reveals that millisecond pulsars will have better SNR at higher frequencies than normal pulsars. It is not easy to evaluate the performance of the UWB receiver to search for pulsars by using PSRPOPPY. We simulated the pulsar searching capability with different center frequencies and bandwidths. In the low Galactic latitude, using the 15 cm receiver from 700 MHz to 2700 MHz, the number of pulsars discovered by simulation is nearly twice that of PAF and 40 cm receivers. However, the survey with 15 cm receiver requires more time and data storage space to complete.

With the 40 cm receiver, about 1000 previously undetected normal pulsars can be discovered in the region $-5^\circ < l < 180^\circ$ and $|b| < 5^\circ$, using 12 minutes per pointing. The survey would take just over 708 days to complete. Using the PAF receiver to survey the same region with 30 minutes per pointing, 2200 previously undetected pulsars can be found in 43 days. Expanding the survey to $|b| < 10^\circ$ will add about 600 unknown pulsars. Considering the influence of scattering, the PAF receiver and 40 cm receiver data rates are 920.3 GB/s and 39.5 GB/s, respectively, when the optimal sub-bandwidth (4.59 kHz and 1.55 kHz) and 8-bit sampling are selected. If only 0.1 MHz is used for the sub-bandwidth, the PAF receiver and 40 cm receiver data rates will be reduced to 42.24 GB/s and 0.612 GB/s, respectively.

Many factors, such as disk space, data rate, and computing resources, need to be considered for the QTT pulsar survey. The optimal observation sub-bandwidth can be determined by the maximum DM in the direction of observation. Compared with a constant channel bandwidth for the survey, the data volume and data rate can be reduced significantly. The observation frequency and bandwidth can be chosen according to the sky background temperature. The PAF receiver is preferred because more sky can be observed with a limited time. It has an excellent performance in searching ordinary pulsars and millisecond pulsars. However, this will also produce a large amount of data in a short time, which is a challenge for data storage and processing. For example, Mode 8 in Table 4 can be completed in 83 days and produce 48 peta-bytes of data. For the eight modes in Table 4, the total amount of data is only related to bandwidth and the time required to complete the survey. Mode 4 can be completed in 3430 days and produce 21 peta-bytes of data. In terms of processing data in real time, the PAF requires at least 675.3 computing resources, the highest of the three receivers. Even with offline processing, the pulsar survey still requires a lot of computing and storage resources.

The receivers can be selected for different sky regions and targets, considering the influence of computing and storage resources. In the region with low sky background radiation, the 40 cm receiver will have a good performance. The 40 cm receiver may be a good choice for target surveys such as unidentified Fermi sources, supernova remnants, and globular clusters in high Galactic latitudes. Then the pulsar search in these regions can be completed in a relatively short time.

Acknowledgements

This work is supported by the National SKA Program of China (No. 2020SKA0120100), the National Natural Science Foundation of China (No. 12041304), the National Key Research and Development Program of China (2017YFA0402600), the Youth Innovation Promotion Association of Chinese Academy of Sciences, the 201* Project of Xinjiang Uygur Autonomous Region of China for Flexibly Fetching in Upscale Talents, the Operation, Maintenance and Upgrading Fund for Astronomical Telescopes and Facility Instruments, budgeted from the Ministry of Finance of China (MOF) and administrated by the Chinese Academy of Sciences (CAS), CAS-MPG LEGACY funding and the Operation. We

thank R. N. Manchester and G. Hobbs for useful comments on this study.

References

Bates, S. D., Lorimer, D. R., Rane, A., & Swiggum, J. 2014, MNRAS, 439, 2893
Bhat, N. D. R., Cordes, J. M., Camilo, F., Nice, D. J., & Lorimer, D. R. 2004, ApJ, 605, 759
Burgay, M., D'Amico, N., Possenti, A., et al. 2003, Natur, 426, 531
Burgay, M., Joshi, B. C., D'Amico, N., et al. 2006, MNRAS, 368, 283
Burgay, M., Keith, M. J., Lorimer, D. R., et al. 2013, MNRAS, 429, 579
Edwards, R. T., Bailes, M., van Straten, W., & Britton, M. C. 2001, MNRAS, 326, 358
Han, J. L., Wang, C., Wang, P. F., et al. 2021, RAA, 21, 107
Hewish, A., Bell, S. J., Pilkington, J. D. H., Scott, P. F., & Collins, R. A. 1968, Natur, 217, 709
Hou, L. G., & Han, J. L. 2014, A&A, 569, A125
Huang, W. J., & Wang, H. G. 2020, ApJ, 905, 144
Jankowski, F., van Straten, W., Keane, E. F., et al. 2018, MNRAS, 473, 4436
Kaspi, V. M., & McLaughlin, M. A. 2004, ApJ, 618, L41
Keane, E., Bhattacharyya, B., Kramer, M., et al. 2015, Advancing Astrophysics with the Square Kilometre Array (AASKA14), 40
Keith, M. J., Jameson, A., van Straten, W., et al. 2010, MNRAS, 409, 619
Krishnakumar, M. A., Mitra, D., Naidu, A., Joshi, B. C., & Manoharan, P. K. 2015, ApJ, 804, 23
Lorimer, D. R., Yates, J. A., Lyne, A. G., & Gould, D. M. 1995, MNRAS, 273, 411
Lorimer, D. R., Faulkner, A. J., Lyne, A. G., et al. 2006, MNRAS, 372, 777
Lyne, A. G., Manchester, R. N., Lorimer, D. R., et al. 1998, MNRAS, 295, 743
Lyne, A. G., Burgay, M., Kramer, M., et al. 2004, Sci, 303, 1153
Ma, J., Pei, X., Wang, N., et al. 2019, SSPMA, 49, 099502
Manchester, R. N., Hobbs, G. B., Teoh, A., & Hobbs, M. 2005, AJ, 129, 1993
Manchester, R. N., Lyne, A. G., D'Amico, N., et al. 1996, MNRAS, 279, 1235
Manchester, R. N., Lyne, A. G., Camilo, F., et al. 2001, MNRAS, 328, 17
Martinez, J. G., Gentile, P., Freire, P. C. C., et al. 2019, ApJ, 881, 166
McLaughlin, M. A., Lyne, A. G., Lorimer, D. R., et al. 2006, Natur, 439, 817
Ransom, S. M., Stairs, I. H., Archibald, A. M., et al. 2014, Natur, 505, 520
Sanidas, S., Cooper, S., Bassa, C. G., et al. 2019, A&A, 626, A104
Stovall, K., Lynch, R. S., Ransom, S. M., et al. 2014, ApJ, 791, 67
Wang, N. 2014, SSPMA, 44, 783
Xie, J., Wang, J., Wang, N., Manchester, R. N., & Hobbs, G. 2022
Yao, J. M., Manchester, R. N., & Wang, N. 2017, ApJ, 835, 29